Climate Dynamics (2020) 54:1897–1911
https://doi.org/10.1007/s00382-019-05092-6

Distinct seasonal climate drivers revealed in a network of tree-ring records from Labrador, Canada

R. Parfitt[1,2] · C. C. Ummenhofer[2] · B. M. Buckley[3] · K. G. Hansen[3] · R. D. D'Arrigo[3]

Received: 28 May 2019 / Accepted: 12 December 2019 / Published online: 2 January 2020

Abstract
Traditionally, high-latitude dendroclimatic studies have focused on measurements of total ring width (RW), with the maximum density of the latewood (MXD) serving as a complementary variable. Whilst MXD has typically improved the strength of the growing season climate connection over that of RW, its measurements are costly and time-consuming. Recently, a less costly and more time-efficient technique to extract density measurements has emerged, based on lignin's propensity to absorb blue light. This Blue Intensity (BI) methodology is based on image analyses of finely-sanded core samples, and the relative ease with which density measurements can be extracted allows for significant increases in spatio-temporal sample depth. While some studies have attempted to combine RW and MXD as predictors for summer temperature reconstructions, here we evaluate a systematic comparison of the climate signal for RW and latewood BI (LWBI) separately, using a recently updated and expanded tree ring database for Labrador, Canada. We demonstrate that while RW responds primarily to climatic drivers earlier in the growing season (January–April), LWBI is more responsive to climate conditions during late spring and summer (May–August). Furthermore, RW appears to be driven primarily by large-scale atmospheric dynamics associated with the Pacific North American pattern, whilst LWBI is more closely associated with local climate conditions, themselves linked to the behaviour of the Atlantic Multidecadal Oscillation. Lastly, we demonstrate that anomalously wide or narrow growth rings consistently respond to the same climate drivers as average growth years, whereas the sensitivity of LWBI to extreme climate conditions appears to be enhanced.

1 Introduction

For climatic studies on multi-decadal to longer timescales, instrumental records are mostly too short to provide sufficiently reliable information for analysis. While Europe and lower- to mid-latitude North America enjoy a relatively dense observational network of high quality station data, remote regions like the subarctic latitudes of North America have very little observational data. As a result, our understanding of multi-decadal or longer-term climate variability over the high latitudes relies on reconstructions of climate from proxy sources and climate models, with tree-ring-derived reconstructions of temperature among the most important sources of climate information. The traditional metric used is total annual ring width (RW), due to the relative ease of processing large numbers of cores samples. Summer temperature is the most commonly reconstructed variable for RW. However, the temperature response of RW has exhibited temporal instability across the high latitudes, known as *divergence* (e.g. D'Arrigo et al. 2008). It has been suggested that such decoupling between temperature and RW may be the result of increased drought stress and evapotranspiration due to temperature exceeding optimum conditions for growth (D'Arrigo et al. 2008; Stine and Huybers 2014). The source of this decoupling is widely considered to be the result of anthropogenic forcing.

Next to RW the second most commonly used tree-ring metric has been maximum latewood density or MXD (expressed as g/cm^3), obtained by soft x-ray of

Electronic supplementary material The online version of this article (https://doi.org/10.1007/s00382-019-05092-6) contains supplementary material, which is available to authorized users.

✉ R. Parfitt
rparfitt@fsu.edu

[1] Department of Earth Ocean and Atmospheric Science, Florida State University, Tallahassee, FL, USA

[2] Department of Physical Oceanography, Woods Hole Oceanographic Institution, Woods Hole, MA, USA

[3] Tree-Ring Laboratory, Lamont-Doherty Earth Observatory of Columbia University, Palisades, NY, USA

thin sections of wood that have been treated to remove all resins and related compounds. The more direct, robust response of MXD to growing season temperature (i.e., summer months), combined with minimal autocorrelation and divergence effects, has made it an appealing alternative option to RW (D'Arrigo et al. 1992). However, the process for obtaining MXD is costly and time consuming and requires very high-quality core samples, thus limiting the number of samples and sites that can be processed. In recent years a new density technique, known as Blue Intensity or BI, has been developed, based on image analyses of the absorption of blue light by lignin in the cells of conifer tracheids (McCarroll et al. 2002; Campbell et al. 2007; Björklund et al. 2013; Rydval et al. 2014; Wilson et al. 2014). Rather than x-raying thin sections, the BI method uses scanned images of resin-extracted wood, and theoretically relies upon lignin's propensity to absorb ultraviolet light more readily than other wood structural components (Fukazawa 1992). Hence a higher degree of reflected blue light indicates lower density (i.e., less lignified wood) and vice versa. In this paper, we make use of a recently updated and expanded tree ring database from Nunatsiavut in Labrador, Canada in order to conduct a systematic comparison of the climate signal for the more traditional RW with the new latewood BI (LWBI) technique separately.

The Labrador tree-ring records are particularly suited for this analysis as they have been shown to reveal important information about the dominant large-scale climate modes that modulate temperature and precipitation across the North Atlantic sector, providing a long-term context for recent and projected climate trends. The ecological vulnerability of this region has considerable implications for indigenous populations via freshwater supply, food sources and ultimately mental health and wellbeing (Goldhar et al. 2014; Macdonald et al. 2015). Rapid warming observed over Labrador over recent decades is likely related to anthropogenic warming. Several unusually warm years appear to be primarily driven by anomalies in North Atlantic sea surface temperatures (SST) and the Arctic Oscillation (Way and Viau 2015). Decreased winter precipitation and the strong summer and fall warming since the early 1990s also seem to have contributed to negative glacier mass balances in northern Labrador (Barrand et al. 2017). More broadly, multi-decadal variations in precipitation over Labrador and Newfoundland appear to be strongly modulated by the North Atlantic Oscillation (NAO) (Banfield and Jacobs 1998; Brown et al. 2012).

The remainder of the paper is structured as follows: Sect. 2 describes the tree-ring data, reanalysis products, and methodology used in this paper. Section 3 presents analysis of the annual and seasonal climatic drivers of RW and latewood BI (LWBI), including a consideration of extreme events, and Sect. 4 offers conclusions.

2 Data and methodology

2.1 Tree ring data

We use an updated and expanded regional tree ring network of white spruce (*Picea glauca*) RW and LWBI time series that were derived from both core and sectional samples. The site locations in Nunatsiavut range from 55° to 58° N latitude (Fig. 1). The core samples included in this study were taken over multiple collection seasons dating back as far as 1986 (D'Arrigo et al. 2003) and as recently as 2017, and here we use regionally averaged records for both RW and LWBI. The sample depth for both records is quite robust, with 416 cores for RW (spanning 1569–2017) and 342 for LWBI (1580–2017). The fidelity of both records is also quite good, with mean series intercorrelation of 0.598 for RW and 0.501 for LWBI. A more complete discussion on the significance of these mean series intercorrelation values is given in Online Resource 1.

2.2 Developing blue intensity data

BI data measurements are inversely correlated with traditional MXD, since dense cell walls express lower reflectance as more blue light is absorbed. We therefore interpret BI as reflecting cell wall density through the amount of lignin in the cells, though other anatomical features are responsible for BI variability as well, such as the lumen diameter. Figure 2 illustrates a direct comparison between MXD and LWBI from an 18-core subset of Labrador spruce cores from the Tree Ring Laboratory at Lamont Doherty Earth Observatory core collection. Assessment of the relationship of both MXD and LWBI with summer temperature using the CRU TS3 v.22 dataset (Harris et al. 2014) for the period 1901–1997, as well as the master dating series indices as calculated from program COFECHA (Holmes 1983) demonstrate that these records are nearly identical. It is noted that the series are shown from 1780 where the sample depth for LWBI reflects at least 4 cores (at least 12 cores from 1800 to 1993) whilst the MXD series represented from 52 to 77 core samples throughout, with the correlation between these two time-series being 0.91. Typically, MXD time series exhibit decreasing trends with increasing age, while for BI the trend increases with age. Traditional methods for detrending time series for dendrochronology within the program ARSTAN (Cook 1985) do not allow positive-linear-only detrending as a standard option, hence BI measurements are inverted to accommodate this detrending option (Björklund et al. 2014, 2015). However, inversion allows BI values to be more easily comparable to MXD, hence for consistency

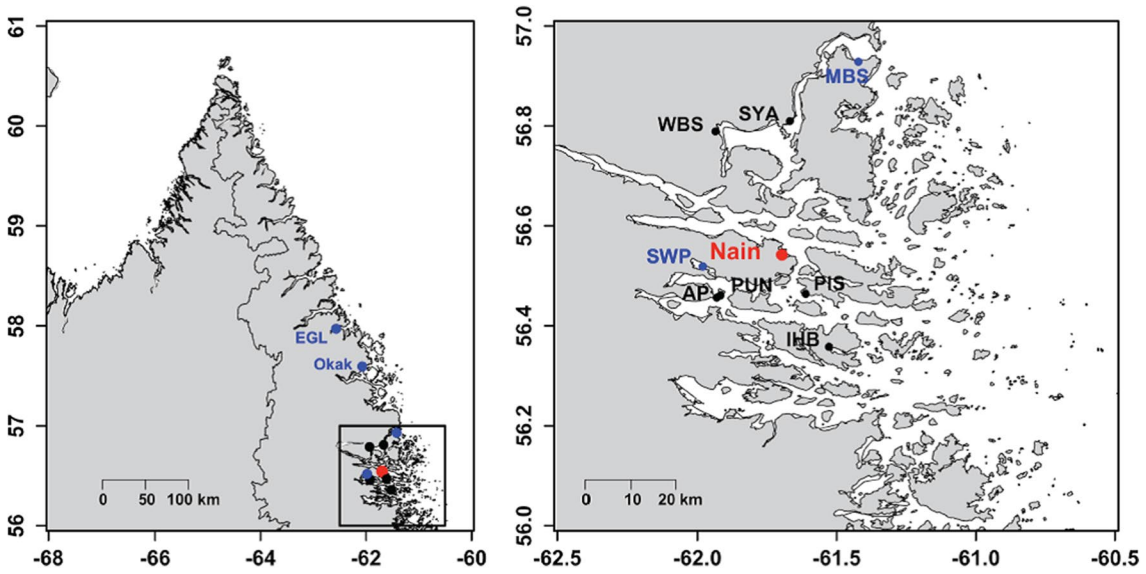

Fig. 1 Map of northern Labrador, Canada, showing the network of white spruce tree-ring sites used in this study (inset box on the left is expanded in the right panel). The sites collected prior to 2017 are shown in blue (*EGL* Eyeglass Lake, *Okak* Okak Bay, *MBS* Medusa Bay, *SWP* Saltwater Pond), while the 2017 collections are shown in black (*WBS* Webb Bay, *SYA* Scratch Yer Arse, *AP* Akuliakatak Peninsula, *PUN* Palungatak Island, *PIS* Paul Island, *IHB* Ittikauk Bay)

with other papers we inverted our data for LWBI (see Rydval et al. 2014) by multiplying each value by − 1 before adding the constant 2.56 to eliminate any negative values. This constant was used because the values are recorded in decimal form with the maximum colour intensity set at 2.56 (i.e., 256 on the colour model described above). Care was taken to ensure that rings denoted as absent for any series (hence given a value of zero) were not corrupted by this procedure, and still retain their original value of zero.

2.3 Standardising growth indices

We used the Signal Free standardisation methodology developed by Melvin and Briffa (2008, 2014) and Briffa and Melvin (2011) to standardise our RW and LWBI time series (shown in Fig. 3), employing RCSig, a freeware program developed at the Lamont-Doherty Earth Observatory based on the commonly used program ARSTAN (Cook 1985). RCSig allows for detrending individual series using methods routinely available in ARSTAN, but within a signal-free framework (see Melvin and Briffa 2008). Using a signal-free framework reduces potential end effect biases that can occur during detrending by removing the common forcing signal within each series (Melvin and Briffa 2008). Accordingly, individual series in our study were detrended using an age-dependent smoothing spline, and the bi-weight robust mean for developing growth indices in order to reduce the effects of outliers (Cook and Kairiukstis 1990). To quantify the signal strength of our record through time we calculated two common statistics, the RBAR and the Expressed Population Signal (EPS) (Wigley et al. 1984). The RBAR metric analyzes the common signal between the available bivariate pairs for any one time, and while its value will not change with sample depth (i.e., N), it will be biased as the relative number of within-tree correlations increases compared to between-tree correlations. In contrast EPS is sensitive to changes in N, as it estimates the hypothetical squared correlation value between the sample chronology and the theoretical infinitely replicated chronology. EPS values that exceed 0.85 are generally considered to demonstrate an acceptable level of common signal fidelity, though there is no actual significance test (Wigley et al. 1984).

2.4 Observational and reanalysis products

The primary reanalysis dataset used in this study is the twentieth Century Reanalysis (20CR) of the National Oceanic and Atmospheric Administration (NOAA) (Compo et al. 2011). The 20CR is an ensemble atmospheric reanalysis extending from 1851 onwards, available daily on a $2^{\circ} \times 2^{\circ}$ longitude-latitude grid, and is developed through assimilation of mean sea-level pressure (MSLP) and monthly sea-surface temperature (SST) and sea-ice conditions. Numerous studies have shown that the 20CR consistently reproduces variability in the Earth system (Peings et al. 2013, Ouzeau et al. 2011). For SST, the Extended Reconstruction Sea-Surface Temperature version 4 (ERSSTv4) dataset (Huang et al. 2014) is used, available monthly from 1854 onwards again on a $2^{\circ} \times 2^{\circ}$ longitude-latitude grid. The main period of analysis considered in this study is 1854–2014. In order to

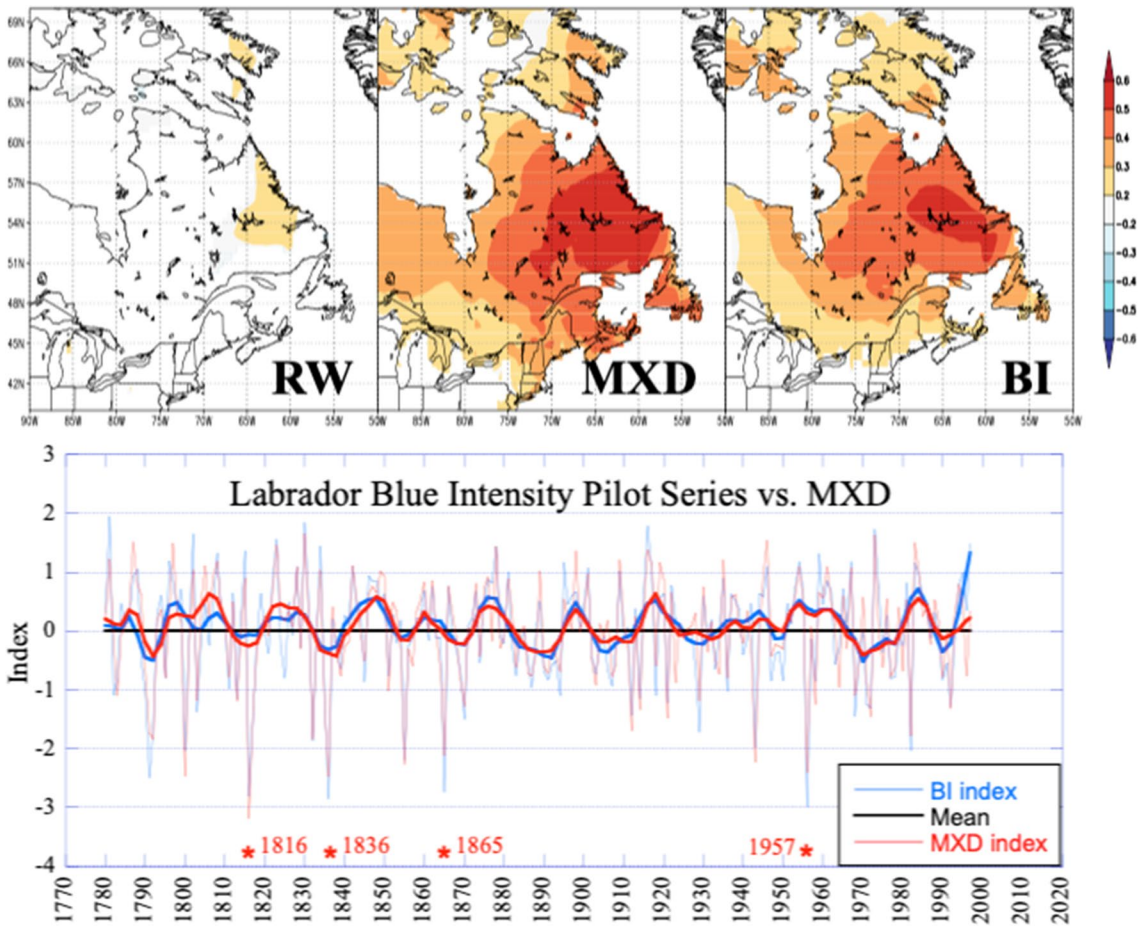

Fig. 2 Proof of concept for latewood Blue Intensity (latewood BI, or LWBI) using 18 white spruce core samples from northern Labrador. The top figures compare the correlation between ring width (RW, top left), maximum density (MXD, top centre) and latewood BI (top right) with summer (June–August) temperature for the period of 1901–1997, in the CRU TS3 v.22 dataset. The lower panel shows the master dating series indices from program COFECHA for the 18-core pilot study for latewood BI from Labrador TRL-LDEO core collection (blue line) against the MXD composite series from the same core collections (red line). Red stars highlight years of major volcanic eruptions

verify the analyses produced using these extended datasets, certain results are also produced using the National Centers for Environmental Prediction Climate Forecast System Reanalysis (NCEP-CFSR) product (Saha et al. 2010) for the period 1979–2010, provided on a 0.5° longitude-latitude grid. Online Resource 2 shows the mean annual precipitation rate as produced from both 20CR and NCEP-CFSR for the period 1979–2010. For the common analysis period 1979–2010, the results in this study are robust across the shorter time period with NCEP-CFSR.

Monthly indices for the Pacific North American pattern and North Atlantic Oscillation are provided by the National Oceanic and Atmospheric Administration Climate Prediction Center (https://www.cpc.ncep.noaa.gov), whilst the Atlantic Multidecadal Oscillation index (calculated as in Trenberth and Shea 2006—see Ting et al. 2009, for discussion regarding alternative definitions) is retrieved from the University Corporation for Atmospheric Research Climate Data Guide (https://climatedataguide.ucar.edu/climate-data/atlantic-multi-decadal-oscillation-amo).

3 Results

First, we systematically assess annual and seasonal climatic conditions that could influence tree-ring growth and how this is reflected in RW and LWBI, respectively.

3.1 Annual long-term correlations

Linear correlation maps between our regional RW and LWBI time series and the detrended annual means for (a) 20CR precipitation rate (b) 20CR mean sea-level pressure (c) 20CR 2-m air temperature and (d) ERSST sea-surface

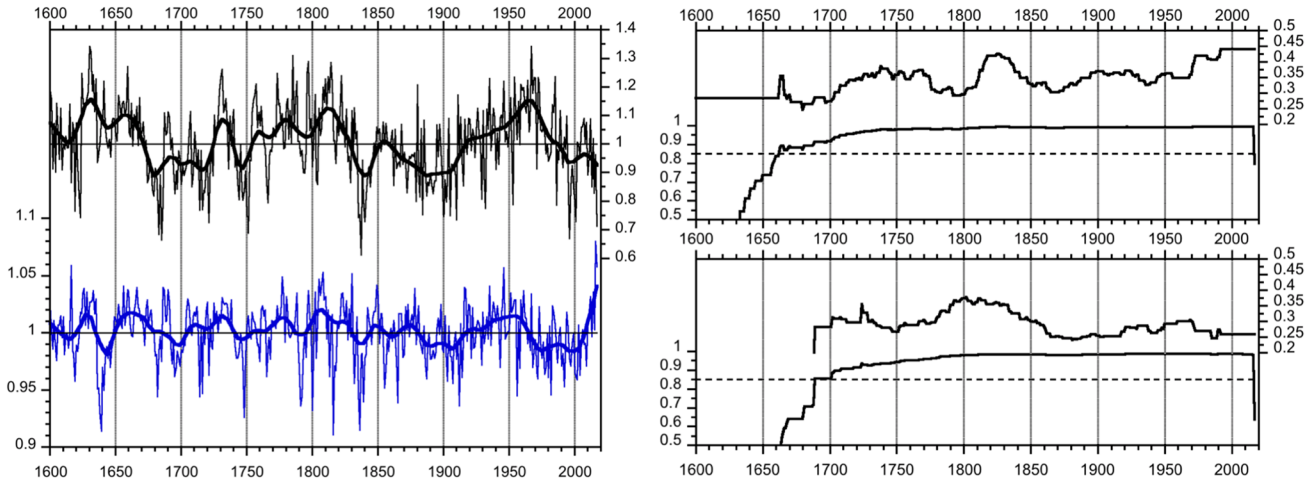

Fig. 3 Master tree-ring indices for Labrador spruce ring width (RW, in black on top left) and Latewood Blue Intensity (LWBI, in blue on the bottom left) for the regionally averaged series described in the text. Both series are represented by more than 400 individual time series at their maxima, and at least 100 time series back as far as the mid-eighteenth century CE. On the right are the RBAR and Expressed Population Signal (EPS) statistics plotted on the top and bottom, respectively, for each record

temperature are shown in Fig. 4. On an annual timescale, RW is correlated with higher (lower) than average precipitation over southern Greenland (northern Canada and the northeastern Pacific). These signals are spatially co-located with lower (higher) than average MSLP signals, indicating a possible dynamic driver for these patterns. Indeed, most precipitation in the mid- to high-latitudes is associated with low-pressure storms and their related fronts (Catto et al. 2012). Furthermore, the spatial pattern of the MSLP correlations resembles the negative phase of the Pacific North American (PNA) pattern (this is considered further in Sect. 3.4), which is known to relate to below-average temperatures over the western United States and Canada (e.g., Leathers et al. 1991). This is somewhat reflected in the annual temperature signal, which exhibits significant negative correlations over the Western United States, but also over Newfoundland local to the tree-ring sites in this study. Negative (positive) correlations with annual SST are observed in Hudson Bay and the Northwestern Passages (the Gulf Stream region off the southeastern seaboard), regions that are known to affect mid-latitude storms (Parfitt et al. 2016). Conversely, for LWBI no significant correlations are observed in the mid-latitude regions for annual precipitation rate or MSLP. However, a significant positive correlation is observed for annual temperature stretching from Newfoundland across the width of the North Atlantic. This signal is spatially accompanied over the ocean by a strong positive correlation with SST. The lack of coherence with precipitation and MSLP suggest that yearly LWBI (i.e., wood density) is not related to a large-scale dynamic driver such as mid-latitude storms, but is instead controlled by the temperature regime regional to the tree-ring sites.

It is noted that in each plot in Fig. 4, correlation significance is identified where the associated p value does not exceed 0.01. Prior research (e.g. Banfield and Jacobs 1998; Way and Viau 2015; Finnis and Bell 2015) however has highlighted that Labrador climate is known to exhibit significant spatial and temporal autocorrelation over annual to decadal timescales, and as such it is important to consider the potential impact of this on significance level. In Sect. 3.2, where we show that these annual correlations associated with the RW and LWBI metrics are heavily seasonally dependent, the potential bias due to spatial and temporal autocorrelation is discussed.

3.2 Seasonal long-term correlations

Given the diverse nature of the annual long-term correlations in Sect. 3.1, it is of interest to comprehensively investigate the seasonal long-term correlations. For example, if RW is intimately related to mid-latitude storms, then one might expect a stronger signal in boreal winter when the storm-tracks and atmospheric fronts are strongest (Chang et al. 2002; Parfitt et al. 2017). To investigate this, three separate periods are considered: January–April, May–August and September–December.

Figure 5 illustrates correlation maps between detrended RW growth data and the detrended January–April means for (a) 20CR precipitation rate (b) 20CR mean sea-level pressure (c) 20CR 2-m air temperature and (d) ERSST sea-surface temperature. For positive RW in January–April, similar signals in precipitation rate are seen as in the annual correlation, augmented by an extended region of lower precipitation across the entirety of Labrador and Newfoundland not

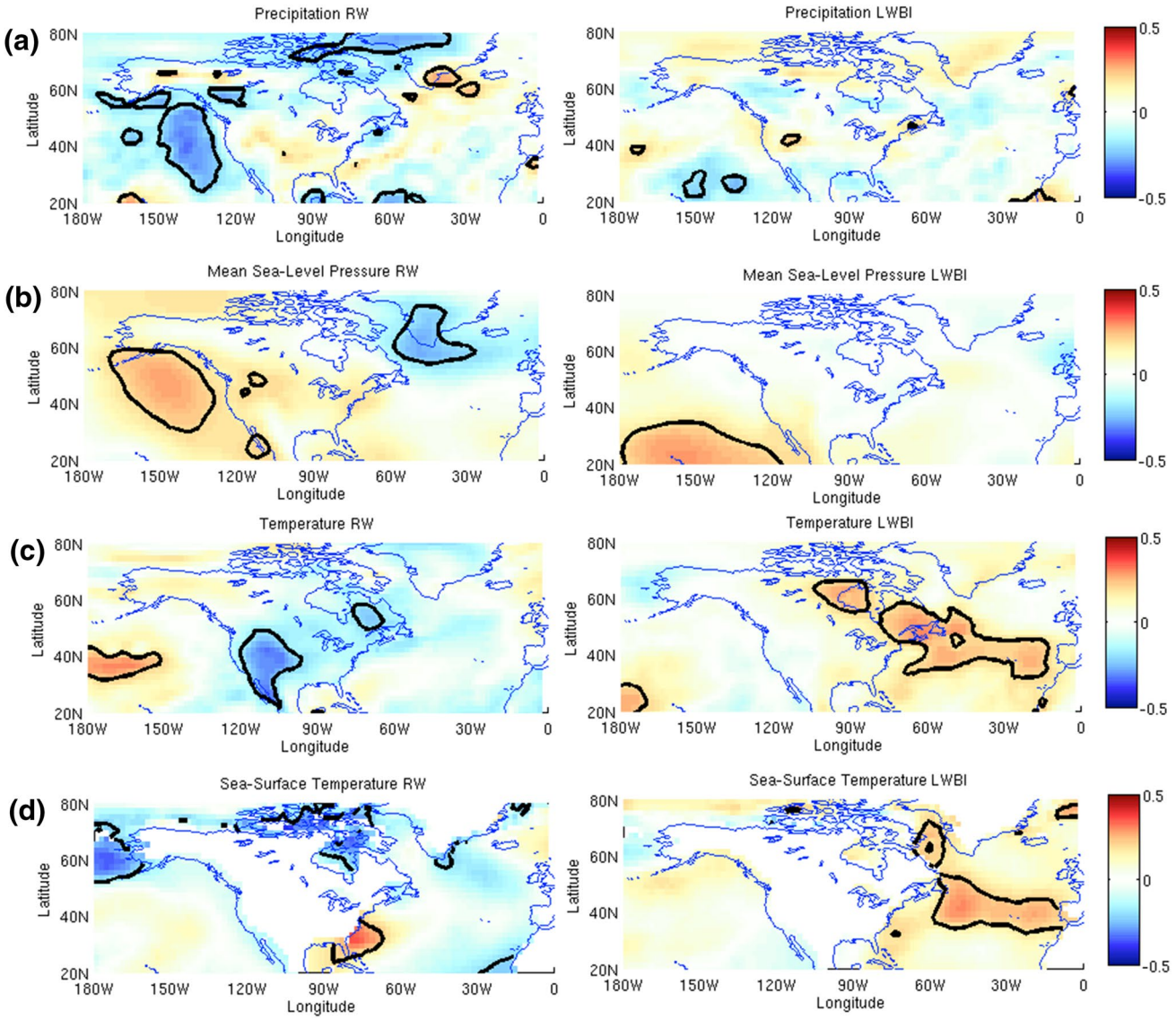

Fig. 4 Correlation maps of detrended RW and LWBI growth time-series with detrended annual averages of **a** 20CR precipitation rate **b** 20CR mean sea-level pressure **c** 20CR 2-m air temperature and **d** ERSST sea-surface temperature. Correlations are shown in colour, with areas denoting significance to $p < 0.01$ illustrated in thick black contours

present in the yearly mean. Spatially, both temperature and MSLP also exhibit a similar signal to the annual correlation, as is the case for the SST. The spatial consistency between precipitation and MSLP once again suggests a large-scale dynamical driver. As the mid-latitude storm-track is strongest in the wintertime, one might indeed expect this degree of consistency to be higher for the January-April season than for the yearly mean. This is considered further in Sect. 3.4. Conversely, in January-April there are negligible correlations between LWBI and either precipitation rate or MSLP, similar to the yearly correlations (Online Resource 3). However, there is also minimal signal for both temperature and SST, except for the Gulf Stream region south of Cape Hatteras. This suggests that the yearly signals seen for LWBI in Fig. 4 are primarily associated with variations later in the year.

Indeed, this is confirmed in the LWBI correlations with May–August means of the variables (Fig. 6). In May–August, there is a strong localised relationship between LWBI and temperature, extending across much of Canada. This is spatially consistent with a significant positive SST correlation off the coast of Newfoundland, suggesting an enhanced role for localised air-sea interactions in summer for impacting LWBI. It is noted that the importance of air-sea interaction for MXD has been previously noted in D'Arrigo et al. (2003), although it was not clear whether this was due to the atmosphere forcing the ocean or vice versa. Furthermore, a broad area of negative MSLP correlation

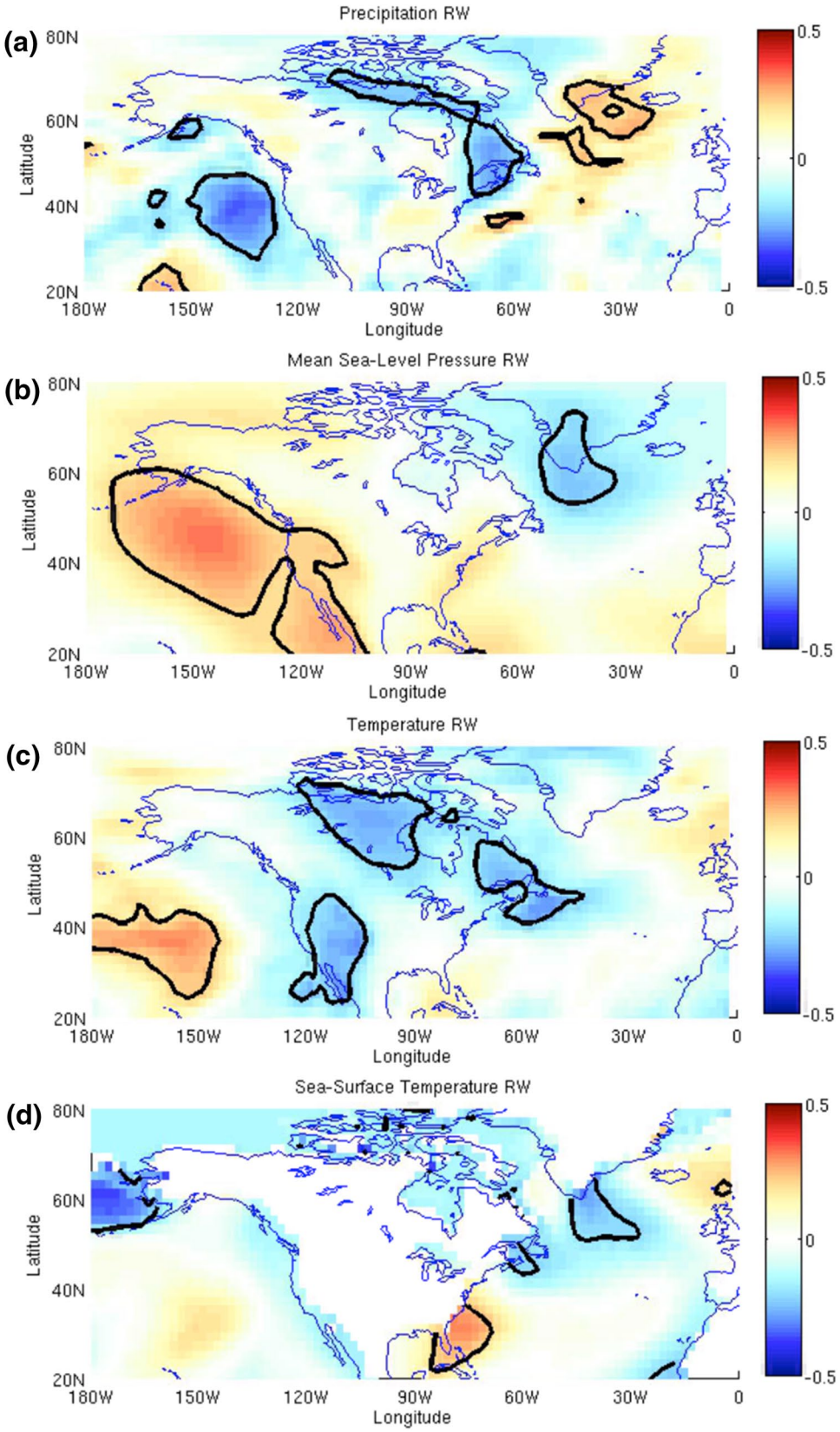

Fig. 5 Correlation maps of detrended RW with detrended January-April averages of **a** 20CR precipitation rate **b** 20CR mean sea-level pressure **c** 20CR 2-m air temperature and **d** ERSST sea-surface temperature. Correlations are shown in colour, with areas denoting significance to $p < 0.01$ illustrated in thick black contours

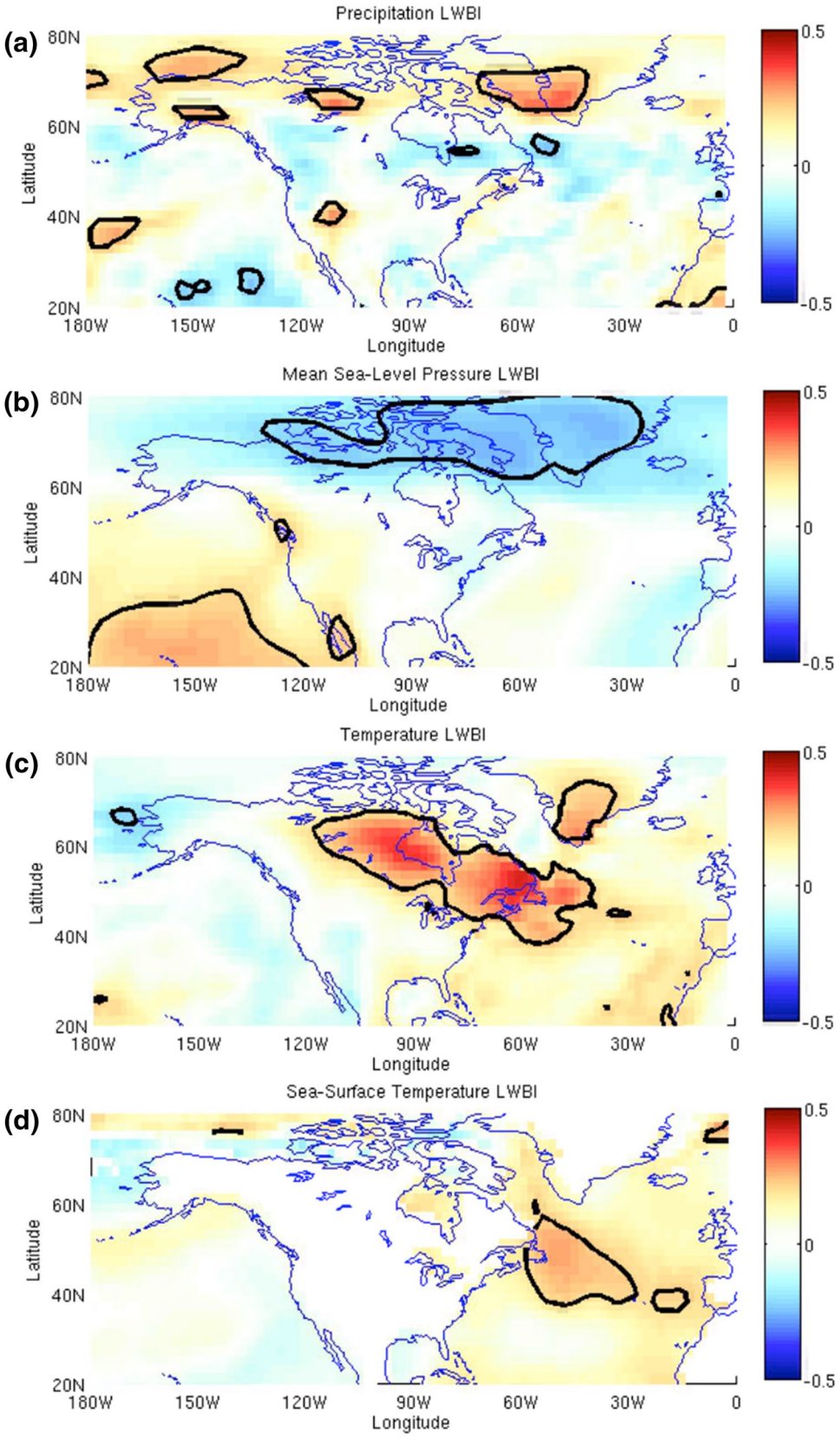

Fig. 6 Correlation maps of detrended LWBI with detrended May–August averages of **a** 20CR precipitation rate **b** 20CR mean sea-level pressure **c** 20CR 2-m air temperature and **d** ERSST sea-surface temperature. Correlations are shown in colour, with areas denoting significance to $p < 0.01$ illustrated in thick black contours

exists across northern Canada and Greenland, suggesting that LWBI is enhanced during periods with low pressures to the north, which may systematically allow for higher temperatures across northeastern North America. For RW in May–August however (Online Resource 4), other than a negative precipitation and MSLP correlation in northern Canada and Greenland, no significant signals are observed.

Given that from September to December, physiological activity in the form of cambial cell formation is negligible, Figs. 5 and 6 suggest that the yearly RW correlations in Fig. 4 are heavily representative of climatic drivers in January–April specifically. In contrast LWBI is primarily correlated with May–August temperatures with little in the way of prior season climate influence. These findings are consistent with prior research that shows RW to have a stronger relationship to prior season climate factors (sensu, Fritts 2012), owing to ecophysiological constraints on tree growth.

Despite the negligible physiological activity, it is nevertheless worth considering the September-December period as any correlations will represent persistence of climatic signals related to growth earlier in the year (January–August). Figure 7 illustrates the correlation maps between detrended RW and LWBI with the detrended September-December means for (a) 20CR 2-m air temperature and (b) ERSST sea-surface temperature. For LWBI, there is a persistence of the same positive temperature and SST seen for May–August in Fig. 6. This suggests that in years of increased wood density (i.e., high LWBI values), summers are both warmer and longer than usual. Furthermore, the positive SST signal extends further poleward into the Labrador Sea, hinting that years with higher LWBI are potentially linked with the delayed onset of Arctic sea-ice. Interestingly, for RW the signal appears to instead be rather opposite: a negative SST correlation in the Northwestern Passages, a signal that is also revealed in the yearly correlations in Fig. 4. Taken together these results suggest one crucial difference between climatic drivers of RW and LWBI, that the former may favour the onset of Arctic sea-ice, whilst the latter is linked to its delayed onset. For both RW and LWBI, there is negligible signal for either precipitation rate or MSLP, as one might expect due to the high level of internal atmospheric variability (Online Resource 5).

3.3 Interpretation of the seasonal long-term correlations

Regarding the correlations in Figs. 4, 5, 6 and 7, it is important to offer several caveats. Firstly, a number of studies have shown 20CR to contain larger biases for certain atmospheric variables at high latitudes (e.g. cloud fraction, Zib et al. 2012). In order to illustrate the robustness of these results to our choice of datasets, the correlations for RW and LWBI are reproduced for both 20CR and NCEP-CFSR for the period 1979–2010 for precipitation rate in January-April (Fig. 8), as well as for both ERSST and NCEP-CFSR for SST in May–August (Online Resource 6). We choose precipitation rate in particular due to the difficulty in its accurate representation in reanalyses, which makes its consistency between datasets harder to capture (e.g. Sun et al. 2018). The comparisons show a high degree of similarity for

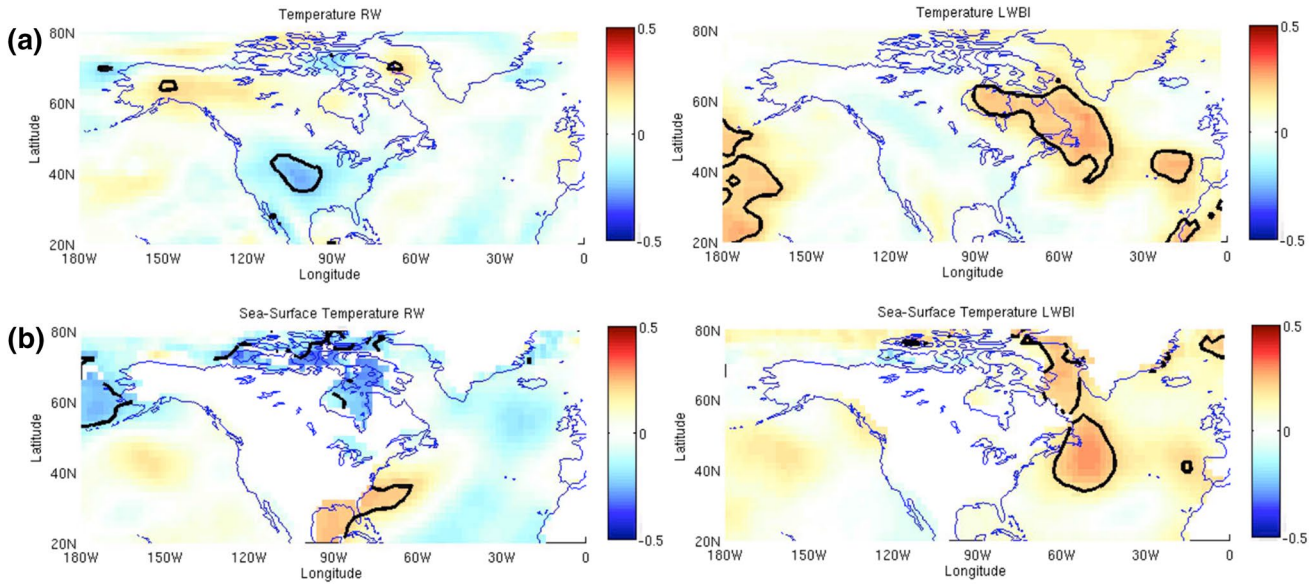

Fig. 7 Correlation maps of detrended RW and LWBI growth time-series with detrended September–December averages of **a** 20CR 2-metre air temperature and **b** ERSST sea-surface temperature. Correlations are shown in colour, with areas denoting significance to $p < 0.01$ illustrated in thick black contours

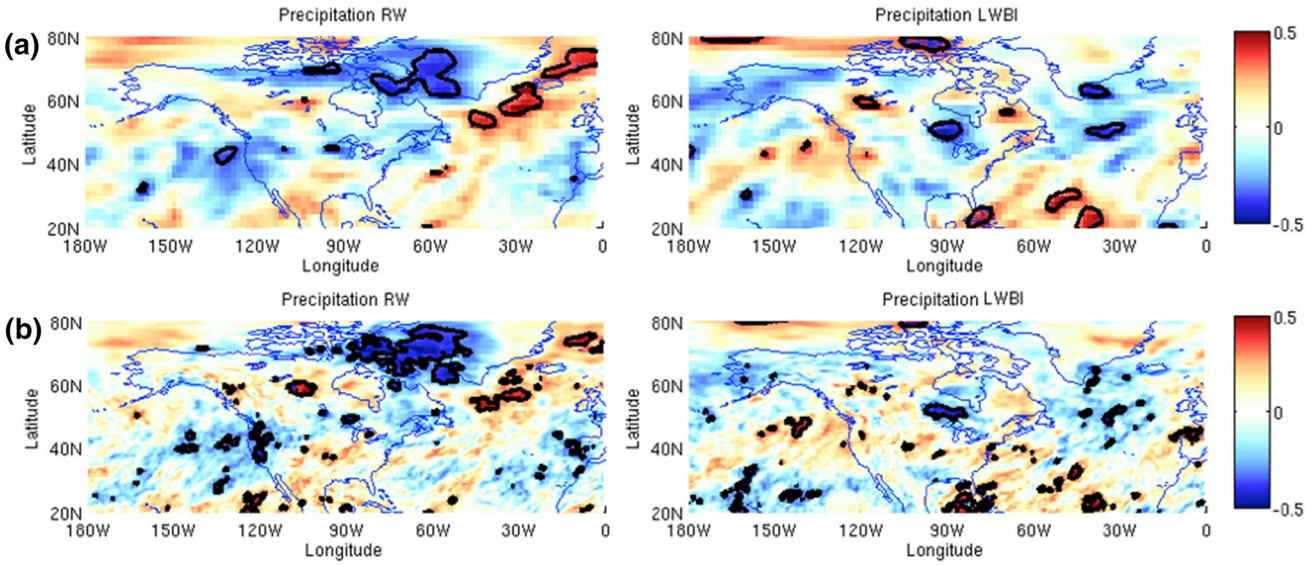

Fig. 8 Correlation maps of detrended RW and LWBI growth time-series with detrended January–April averages of precipitation rate in **a** 20CR and **b** NCEP-CFSR, for the period 1979–2010. Correlations are shown in colour, with areas denoting significance to $p < 0.05$ illustrated in thick black contours

both precipitation rate and SST, providing confidence in the choice of datasets for this analysis. It is interesting to note that the magnitude of the identified correlations is stronger for the period 1979–2010 than for the full 1854–2014 period. One possibility is that reanalyses are more accurately constrained in recent years due to the availability of observations, which may potentially lead to stronger relationships between tree-ring metrics and climatic variables. If so, it is possible that the signals identified within this study may be underestimated.

Secondly, as aforementioned, several studies such as Finnis and Bell (2015) note that significant spatial and temporal autocorrelation exists in relation to Labrador climate. As such, it is important to address this in relation to Figs. 4, 5, 6, 7 and 8 to avoid unintentionally overstating the significance of the identified correlations. To test the potential impact of spatial autocorrelation, a point representative of the Labrador tree-ring sites is selected, (62 W, 58 N), and the anomalies in MSLP, temperature and precipitation identified there in January–April are correlated against MSLP, temperature and precipitation anomalies respectively at all other locations (Online Resource 7). In both periods, high spatial autocorrelations ($r > 0.8$) in all variables are identified within a localised point radius of ~ 500–1000 km specifically. These results suggest that any significant correlations identified between RW or LWBI and the aforementioned variables in the immediate area neighbouring the tree-ring sites must be considered with caution, due to the correlated variables at those locations not being sufficiently independent of one another. Comparison however with Fig. 5 illustrate that the January-April signals discussed in Sect. 3.2 mostly extend well beyond these regions of high spatial-autocorrelation. This is also the case in both May–August and September–December (not shown). To test the potential impact of temporal autocorrelation, Durbin–Watson (Durbin and Watson 1951; Farebrother 1980) and associated tests were applied at multiple locations in Figs. 4, 5, 6, 7 and 8 where statistically significant relationships were identified. For the relationships between RW or LWBI with each atmospheric variable, as well as that between LWBI and SST, temporal autocorrelation did not appear to influence the identified statistical significance at any location. Whilst also true at most locations tested for those identified between RW and SST however, it is noted that at several grid points the tests suggested that the p-values for the correlations between RW and SST specifically may potentially be overstated.

3.4 Relation to climate indices

In Sects. 3.1 and 3.2, the seasonal correlations between tree-ring growth anomalies and precipitation, MSLP, temperature and SST hinted at the possibility of large-scale dynamic drivers. It therefore makes sense to analyse the relationship between tree-ring growth anomalies and well-known modes of mid-latitude climate variability that affect North American climate. We first consider the PNA pattern, one of the prominent modes of variability in the Northern Hemisphere mid-latitudes, from 1950 to 2014. In Sects. 3.1 and 3.2, we noted certain similarities between known PNA patterns and RW correlations, along with discussion on the dynamic coherence between precipitation and MSLP. Indeed, the PNA is known dynamically to affect the East

Asian jet exit region towards the western United States. Figure 9a illustrates the correlation coefficients of RW (red) and LWBI (blue) anomalies with annual and seasonal PNA indices. For LWBI, both annually and seasonally there is an insignificant relationship with the PNA. However, for RW there is a correlation coefficient of −0.38 (p-value < 0.01) with the PNA in January-April. Indeed, on any timescale −0.38 is relatively high for a correlation with a teleconnection pattern and suggests that yearly RW can offer a reasonable indication of PNA phase in January–April (and hence also of the temperature patterns across much of northern North America). For annual means this relationship between RW and the PNA drops to −0.23, and is reflective of the non-significant correlations found later in the year (0.16 in May–August and −0.17 in September–December). Figure 9a, combined with Figs. 4, 5, 6, 7, strongly suggests that RW in any given year is linked to large-scale Northern Hemispheric winter dynamics at the start of the year. Consideration of the spatial autocorrelation between the PNA index and January–April anomalies in temperature, MSLP and precipitation local to the Labrador tree-ring sites (not shown) suggest this relationship to be robust. Similar tests to those discussed in Sect. 3.3 were also used to confirm that temporal autocorrelation in either the RW or PNA indices is not expected to impact the statistical significance of the identified relationship.

To further investigate the dynamics relating to tree-ring growth, the NAO from 1950 to 2014 is considered (Fig. 9b), as it is the dominant mode of winter climate variability in the North Atlantic from central North America into Europe and has been considered in the context of Labrador climate in previous studies (e.g. Finnis and Bell 2015). However, for both RW and LWBI, correlations both annually and seasonally are extremely low (< 0.10 in magnitude), suggesting that the NAO does not play an influential role. This is perhaps due to the considerable non-stationarity of the NAO over time to regional climate which has proven a challenge for tree-ring based reconstructions of the NAO in North Atlantic rim countries in the past. Given that the PNA is closely associated with fluctuations in the East Asian jet stream, this low correlation with the NAO perhaps hints that the dynamic forcing for RW across Labrador arrives from the Pacific. Indeed, there has been recent precedent in paleoclimate studies that are suggestive of strong Pacific influences over ecological processes in the Northwestern Atlantic (Wanamaker et al. 2018).

Lastly, due to significant SST correlations across the North Atlantic with LWBI, we consider the Atlantic Multidecadal Oscillation (AMO) Index from 1950 to 2014 (Fig. 9c). Here we calculate the AMO as in Trenberth and Shea (2006), with global mean SST time-series subtracted from each grid box prior to averaging the SSTs over the AMO region to remove a uniform warming signal. Indeed,

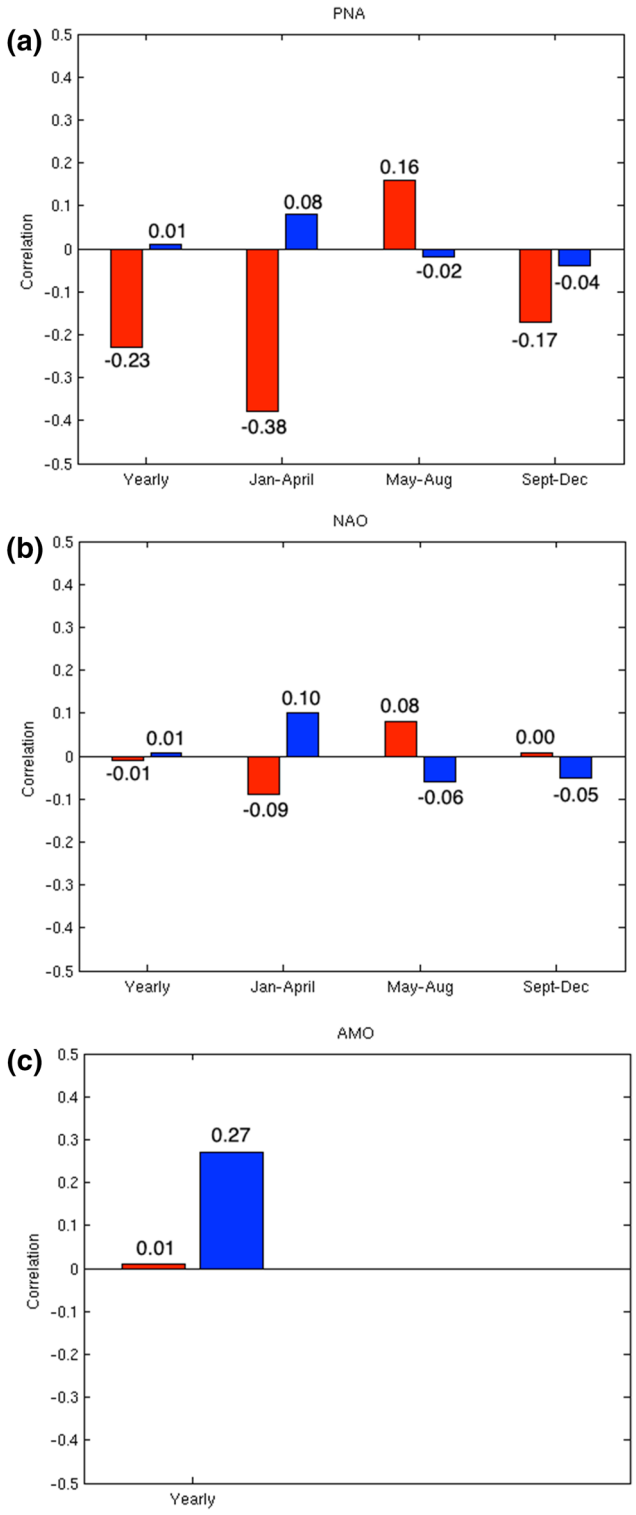

Fig. 9 Correlation coefficients between detrended RW (red) and LWBI (blue) growth time-series with the **a** annualised and seasonal Pacific North American pattern indices for the period 1950–2014 **b** annualised and seasonal North Atlantic Oscillation indices for the period 1950–2014 and **c** Atlantic Multidecadal Oscillation index for 1950–2014, with warming trends removed (Trenberth and Shea 2006)

a correlation coefficient of 0.27 (p-value < 0.01) is identified for LWBI, suggesting the influence of North Atlantic SST variability. This, combined with the spatially coherent temperature and SST influence in May–August (Fig. 6), suggests a role for boreal summer local air-sea interaction processes in driving yearly LWBI, while for RW the correlation is negligible. It is noted that the same correlation coefficient of 0.27 (p-value < 0.01) between LWBI and the AMO index is identified if the period considered is 1854–2014 instead.

3.5 Drivers of extreme tree-ring growth

In Sects. 3.1 and 3.2, it was shown that on average RW and LWBI respond differently in both the nature and seasonality of their long-term climatic drivers, providing motivation for considering RW and LWBI indices separately. This also opens up the question as to whether the climate drivers are the same for extreme RW and LWBI values as they are on average (as considered in Sects. 3.1 and 3.2). For this reason, composites of the previously analysed variables are considered for the 10 years between 1854 and 2014 where RW and LWBI each exhibit maximum growth. It is noted that three out of the 10 years for both maximum RW and LWBI are the same, emphasising that despite the different seasonal drivers, there is nevertheless an underlying relationship between the two indices. Indeed, the correlation between the detrended RW and LWBI indices for the period used in this study is 0.31. It is noted that for better comparison between seasons, the data used in these composites are not just detrended but also have the long-term seasonal means removed.

Figure 10 illustrates the composites in January-April for anomalies in (a) 20CR precipitation rate (b) 20CR mean sea-level pressure (c) 20CR 2-m air temperature and (d) ERSST sea-surface temperature, for maximum RW and LWBI values. For RW, there is a high degree of similarity in the anomalous patterns in MSLP and precipitation with the correlations in Fig. 5, suggesting in January–April that the climatic drivers for extreme RW values are not different to those driving RW values on average. One noticeable difference, however, is the large and statistically significant negative signal in SST over the western North Atlantic, suggesting that the oceanic relationship with extreme January–April RW growth is in fact distinct to that observed on average. Interestingly, despite Online Resource 3 suggesting that on average LWBI is unresponsive to climate drivers in January-April, Fig. 10 shows striking significant MSLP signals of similar magnitude to those for RW. One possibility is that years of high LWBI have a certain dynamical pre-conditioning. For example, the increased poleward heat transport associated with the low-pressure anomaly in Jan-April centred over the United States may create favourable conditions for the development of the strongest high temperature anomalies over Newfoundland in May–Aug, which in turn results in increases in lignification for Labrador spruce trees.

Overall, comparison of Figs. 5 and 10 suggest that for RW regions of strong correlation in seasonal averages are in general also observed for maximum growth, with the exception of the strong SST anomalies in the North Atlantic present for maximum RW growth. This suggests that climatic drivers of RW are similar for both average and extreme conditions. For LWBI however, the differences are more striking, hinting that extremely large LWBI values may reflect climatic conditions rather differently to those on average.

Consideration of the similar composites for May–August (Online Resource 8) and September–December (Online Resource 9) indeed confirm that climatic drivers of RW are similar to those on average, except for the presence of a large negative SST anomaly in the North Atlantic. For LWBI however, the differences are even more noticeable than for January–April. Specifically, extremely large LWBI values are sensitive specifically to local temperature and SST conditions that persist through to the end of the year, suggesting that localised air-sea interaction in the context of oceanic heat input into the atmosphere is especially critical in modulating the strongest lignification processes in spruce trees.

Lastly, the fact that climatic drivers of RW are similar for both average and extreme scenarios, whilst extremely large LWBI values reflect climatic conditions rather differently to those on average, can be further highlighted through testing the sensitivity of the composite sample size, i.e. how many years contribute to the composite maximum. Online Resource 10 illustrates the same as Fig. 10 except for a composite sample size of 16 instead of 10 is used. Whilst the signals for RW remain similar to Fig. 10, those for LWBI are noticeably different in that they no longer exhibit any significant anomalies, i.e. more like the average January–April correlations with LWBI on average shown in Online Resource 3.

For reference, anomaly plots for minimum values in RW and LWBI for January–April, May–August and September-December are also provided in Online Resources 11, 12 and 13, respectively.

4 Conclusions

In recent years, advances in the measurement and processing of tree-ring density, via the more cost effective and less time consuming BI methodology, has allowed for density data of comparable size to traditional ring-width measurements. In particular, pioneering work has led to substantial collocated records from across the northernmost forests of Labrador, a region of significant climatic importance and one that exhibits substantial variability on all timescales.

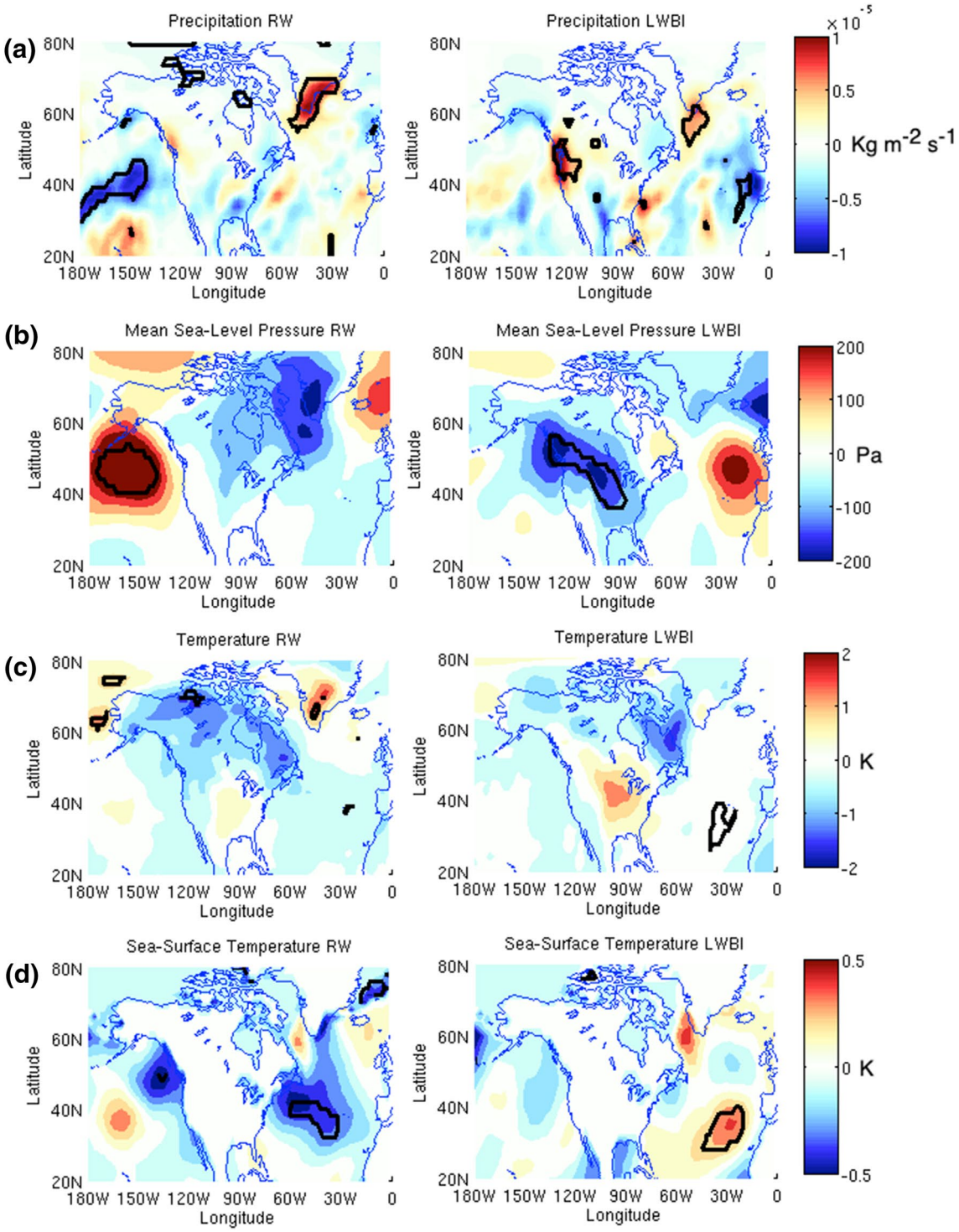

Fig. 10 Composites of anomalies in January-April in **a** 20CR precipitation rate **b** 20CR mean sea-level pressure **c** 20CR 2-m air temperature and **d** ERSST sea-surface temperature, identified for the set of 10 years where (i) RW and (ii) LWBI exhibited maximum growth in the period 1854–2014. For RW, these years were 1880, 1935, 1946, 1954, 1959, 1967, 1969, 1970, 1972 and 1985. For LWBI, these years were 1878, 1916, 1917, 1935, 1946, 1961, 1967, 1983, 2012 and 2014. Black contours mark where the two-sample t-test indicates significance at the 0.05 level

Taking advantage of these records, this study has attempted to be the first to present a comprehensive study of both inter- and intra- annual climatic influences on both RW and LWBI metrics separately. In doing so we identify substantial differences between RW and LWBI in terms of their association with the state of the atmosphere and sea-surface. On average, whilst LWBI is more responsive to local temperature and SSTs in the late spring/summer (a finding consistent with previous studies), RW primarily responds to large-scale atmospheric conditions early in the year. The importance of this finding lies with the general impression in the dendroclimatic community that density offers an improvement over RW precisely because of its direct and more easily interpreted response to local temperature.

RW studies have been plagued by the divergence issue, owing to non-linearity in the response to temperature, and here we show that the RW climate connection is in fact more deeply connected to dynamical processes that are not easily identified by simple correlation with temperature. Indeed, our seasonal analyses here illustrate that RW may in fact offer climatic information of greater importance, dynamically speaking, than regional temperature. This is highlighted through further analysis of RW and LWBI data with common modes of climate variability known to impact the northwestern Atlantic. It is found that there is a strong relationship between RW in January-April and the PNA. Interestingly, no relationship is identified between RW and the NAO or AMO, perhaps suggesting a more influential role for the Pacific in forcing RW growth in Newfoundland and Labrador. Whilst no relationship is found between LWBI and the PNA and NAO, a reasonable correlation is identified for the AMO, emphasising the importance of local SSTs in modulating air-sea interaction and contributing to the local temperature signals influencing growth in May–August.

Interestingly, analysis for the September-December season (when physiological dormancy is initiated) also shows some significant features of note, in particular for SST. For LWBI, in addition to a local persistence of positive temperature and SST anomalies, there is an extension of positive SSTs into the northern Labrador Sea, whilst for RW there is a significant negative SST signal in the Northwestern Passages. This suggests that situations driving RW and LWBI earlier in the year may in some way pre-condition the atmosphere and ocean in a manner that impacts the onset of Arctic sea-ice in the ensuing winter.

Lastly, it is found that extremes in RW growth generally exhibit similar climatic drivers to those observed for growth on average. However, numerous differences are identified for the largest LWBI values. In particular, statistically significant sizeable MSLP anomalies are observed in January–April for years of the largest LWBI values that are not present in long-term seasonal averages. This suggests that in these cases LWBI (i.e., the lignification process that serves to protect tracheid cells from freeze damage during dormancy) may be triggered by certain climatic conditions that differ from those that traditionally drive modest LWBI values. Furthermore, for extreme maxima in both RW and LWBI, significant SST anomalies indicate a much closer relationship with the ocean than on average. Currently, research more acutely investigating the relationship between oceanic variability and RW and LWBI time-series is being undertaken by the authors.

Acknowledgements Observational and reanalysis products were provided by NOAA/OAR/ESRL PSD, Boulder, Colorado, through their website http://www.cdc.noaa.gov, and NERC/NCAS, UK, through the website https://crudata.uea.ac.uk/cru/data/hrg/. In particular, use of the following data sets is gratefully acknowledged: NOAA ERSST v4; 20CR Project supported by the U.S. Department of Energy, Office of Science Innovative and Novel Computational Impact on Theory and Experiment program, and Office of Biological and Environmental Research, and by the NOAA Climate Program Office; NCEP-CFSR data developed by NOAA's NCEP and provided through the Research Data Archive, which is maintained by the Computational and Information Systems Laboratory (CISL) at NCAR, sponsored by the National Science Foundation (NSF); CRU TS3 v.22 dataset supported by NERC. An index for the Atlantic Multidecadal Oscillation was provided by the University Corporation for Atmospheric Research Climate Data Guide, whilst the Pacific North American and North Atlantic Oscillation indices were provided by the NOAA Climate Prediction Center. The authors wish to thank our colleagues and friends in Labrador, in particular Henry, Ches and Joe Webb, for their tireless assistance in our field sampling expeditions. This research was supported by NSF through AGS-1602009. The helpful comments of two anonymous reviewers in improving this manuscript are acknowledged.

References

Banfield CE, Jacobs JD (1998) Regional patterns of temperature and precipitation for Newfoundland and Labrador during the past century. Can Geogr 42:354–364

Barrand NE, Way RG, Bell T, Sharp MJ (2017) Recent changes in area and thickness of Torngat Mountain glaciers (northern Labrador, Canada). The Cryosphere 11:157–168

Björklund JA, Gunnarson BE, Seftigen K, Esper J, Linderholm HW (2013) Is Blue Intensity ready to replace maximum latewood density as a strong temperature proxy? A tree-ring case study on Scots pine from northern Sweden. Clim Past Discuss 9:5227–5261

Björklund JA, Gunnarson BE, Seftigen K, Esper J, Linderholm HW (2014) Blue intensity and density from northern Fennoscandian tree rings, exploring the potential to improve summer temperature reconstructions with earlywood information. Clim Past 10:877–885

Björklund J, Gunnarson BE, Seftigen K, Zhang P, Linderholm HW (2015) Using adjusted Blue Intensity data to attain high-quality summer temperature information: a case study from Central Scandinavia. The Holocene 25:547–556

Briffa KR, Melvin TM (2011) A closer look at regional curve standardization of tree- ring records: justification of the need, a warning of some pitfalls, and suggested improvements in its application. In: Hughes MK, Swetnam TW, Diaz HF (eds) Dendroclimatology. Springer, Dordrecht, pp 113–145

Brown R, Lemay M, Allard M, Barrand NE, Barrette C, Bégin Y, Dibike Y (2012) Climate variability and change in the Canadian

Eastern Subarctic IRIS region (Nunavik and Nunatsiavut). Nunavik and Nunatsiavut: From science to policy. An Integrated Regional Impact Study (IRIS) of climate change and modernization, pp 57–93
Campbell R, McCarroll D, Loader N, Grudd H, Robertson I, Jalkanen R (2007) Blue intensity in *Pinus sylvestris* tree rings: developing a new palaeoclimate proxy. The Holocene 17:821–828
Catto JL, Jakob C, Berry G, Nicholls N (2012) Relating global precipitation to atmospheric fronts. Geophys Res Lett 39(L10):805. https://doi.org/10.1029/2012GL051736
Chang EK, Lee S, Swanson KL (2002) Storm track dynamics. J Clim 15(16):2163–2183
Compo GP, Whitaker JS, Sardeshmukh PD, Matsui N, Allan RJ, Yin X, Brönnimann S (2011) The twentieth century reanalysis project. Q J R Meteorol Soc 137(654):1–28
Cook ER (1985) A time series analysis approach to tree-ring standardization. Ph.D. Dissertation, University of Arizona, Tucson, p 171
Cook ER, Kairiukstis L (1990) Methods of dendrochronology. Springer, New York
D'Arrigo R, Jacoby GC, Free RM (1992) Tree-ring width and maximum latewood density at the North American tree line: parameters of climatic change. Can J For Res 22(9):1290–1296
D'Arrigo R, Buckley B, Kaplan S (2003) Interannual to multidecadal modes of Labrador climate variability inferred from tree rings. Clim Dyn 20:219–228
D'Arrigo R, Wilson R, Liepert B, Cherubini P (2008) On the 'divergence problem' in northern forests: a review of the tree-ring evidence and possible causes. Glob Planet Change 60(3–4):289–305
Durbin J, Watson GS (1951) Testing for serial correlation in least squares regression. II. Biometrika 38(1/2):159–177
Farebrother RW (1980) The Durbin-Watson test for serial correlation when there is no intercept in the regression. Econometrica 48:1553–1563
Finnis J, Bell T (2015) An analysis of recent observed climate trends and variability in Labrador. Can Geographer/Le Géogr Can 59(2):151–166
Fritts HC (2012) Tree rings and climate. Elsevier, Amsterdam
Fukazawa K (1992) Ultraviolet microscopy. In: Lin SY, Dence CW (eds) Methods in lignin chemistry. Springer, Berlin, pp 110–121
Goldhar C, Bell T, Wolf J (2014) Vulnerability to freshwater changes in the Inuit settlement region of Nunatsiavut, Labrador: a case study from Rigolet. Arctic 67:71–83
Harris I, Jones PD, Osborn TJ, Lister DH (2014) Updated high-resolution grids of monthly climatic observations - the CRU TS3.10 Dataset. Int J Climatol 34:623–642
Holmes RL (1983) Computer-assisted quality control in tree-ring dating and measurement. Tree Ring Bull 43:69–77
Huang B, Banzon VF, Freeman E, Lawrimore J, Liu W, Peterson TC, Smith TM, Thorne PW, Woodruff SD, Zhang H-M (2014) Extended Reconstructed Sea Surface Temperature version 4 (ERSST.v4): part I. Upgrades and intercomparisons. J Clim 28:911–930
Leathers DJ, Yarnal B, Palecki MA (1991) The Pacific/North American teleconnection pattern and United States climate. Part I: regional temperature and precipitation associations. J. Clim 4:517–528
Macdonald JP, Willox AC, Ford JD, Shiwak I, Wood M, IMHACC Team, and the Rigolet Inuit Community Government (2015) Protective factors for mental health and well-being in a changing climate: perspectives from Inuit youth in Nunatsiavut, Labrador. Soc Sci Med 141:133–141
McCarroll D, Pettigrew E, Luckman A (2002) Blue reflectance provides a surrogate for latewood density of high-latitude pine tree rings. Arct Antarct Alp Res 34:450–453
Melvin TM, Briffa KR (2008) A "signal-free" approach to dendroclimatic standardisation. Dendrochronologia 26(2):71–86
Melvin TM, Briffa KR (2014) CRUST: software for the implementation of regional chronology standardisation: part 1. Signal-free RCS. Dendrochronologia 32(1):7–20
Ouzeau G, Cattiaux J, Douville H, Ribes A, Saint-Martin D (2011) European cold winter 2009/10: how unusual in the instrumental record and how reproducible in the Arpege-Climate model? Geophys Res Lett 38:L11706. https://doi.org/10.1029/2011GL047667
Parfitt R, Czaja A, Minobe S, Kuwano-Yoshida A (2016) The atmospheric frontal response to SST perturbations in the Gulf Stream region. Geophys Res Lett 43(5):2299–2306
Parfitt R, Czaja A, Seo H (2017) A simple diagnostic for the detection of atmospheric fronts. Geophys Res Lett 44(9):4351–4358
Peings Y, Brun E, Mauvais V, Douville H (2013) How stationary is the relationship between Siberian snow and Arctic Oscillation over the 20th century? Geophys Res Lett 40:183–188
Rydval M, Larsson L-Å, McGlynn L, Gunnarson BE, Loader NJ, Young GHF, Wilson R (2014) Blue intensity for dendroclimatology: should we have the blues? Experiments from Scotland. Dendrochronologia 32:191–204
Saha S, Moorthi S, Pan HL, Wu X, Wang J, Nadiga S, Liu H (2010) The NCEP climate forecast system reanalysis. Bull Am Meteor Soc 91(8):1015–1058
Stine AR, Huybers P (2014) Arctic tree rings as recorders of variations in light availability. Nat Commun 5:3836
Sun Q, Miao C, Duan Q, Ashouri H, Sorooshian S, Hsu KL (2018) A review of global precipitation data sets: data sources, estimation, and intercomparisons. Rev Geophys 56(1):79–107
Ting M, Kushnir Y, Seager R, Li C (2009) Forced and internal twentieth-century SST trends in the North Atlantic. J Clim 22(6):1469–1481
Trenberth KE, Shea DJ (2006) Atlantic hurricanes and natural variability in 2005. Geophys Res Lett 33:1–4
Wanamaker AD, Griffin SM, Ummenhofer CC, Whitney NM, Black B, Parfitt R, Kreutz KJ (2018) Pacific climate influences on ocean conditions and extreme shell growth events in the Northwestern Atlantic (Gulf of Maine). Clim Dyn. https://doi.org/10.1007/s00382-018-4513-8
Way RG, Viau AE (2015) Natural and forced air temperature variability in the Labrador region of Canada during the past century. Theor Appl Climatol 121:413–424
Wigley TM, Briffa KR, Jones PD (1984) On the average value of correlated time series, with applications in dendroclimatology and hydrometeorology. J Clim Appl Meteorol 23:201–213
Wilson R, Rao R, Rydval M, Wood C, Larsson LÅ, Luckman BH (2014) Blue Intensity for dendroclimatology: the BC blues: a case study from British Columbia, Canada. The Holocene 24:1428–1438
Zib BJ, Dong X, Xi B, Kennedy A (2012) Evaluation and intercomparison of cloud fraction and radiative fluxes in recent reanalyses over the Arctic using BSRN surface observations. J Clim 25(7):2291–2305